





Diffraction-based overlay metrology from visible to infrared wavelengths using a single sensor

Theodorus T. M. van Schaijk ^{a,b,*} Christos Messinis ^{a,b} Nitesh Pandey,^c
Armand Koolen ^{b,c}, Stefan Witte,^{a,b} Johannes F. de Boer ^b
and Arie den Boef^{a,b,c}

^aAdvanced Research Center for Nanolithography, Computational Imaging Group,
Amsterdam, The Netherlands

^bVrije Universiteit Amsterdam, LaserLaB, Amsterdam, The Netherlands

^cASML, Veldhoven, The Netherlands

Abstract

Background: Integrated circuits are fabricated layer by layer. It is crucial to their performance that these layers are well aligned to each other, and any undesired translation of a layer is called overlay. Thus far, overlay measurements have been limited to visible wavelengths, but the use of materials that are opaque to visible wavelengths necessitates measurements using infrared light.

Aim: We set out to demonstrate that an overlay sensor based on digital holographic microscopy can perform such overlay measurement at infrared wavelengths, while maintaining functionality at visible wavelengths.

Approach: This was done by constructing a breadboard setup that is capable of measuring overlay at wavelengths ranging from 400 to 1100 nm.

Results: Using the setup, we demonstrated good linearity between an applied amount of overlay and the measured amount. In addition, we demonstrated that the setup is only sensitive to structures at the top of the wafer. Measurements are therefore unaffected by the fact that Si is transparent at 1100 nm.

Conclusions: These results demonstrate the viability of an overlay sensor that is sensitive to visible and infrared light, allowing more freedom in choice of materials for integrated circuits.

© The Authors. Published by SPIE under a Creative Commons Attribution 4.0 International License. Distribution or reproduction of this work in whole or in part requires full attribution of the original publication, including its DOI. [DOI: [10.1117/1.JMM.21.1.014001](https://doi.org/10.1117/1.JMM.21.1.014001)]

Keywords: overlay metrology; dark-field microscopy; digital holographic microscopy; broadband imaging; infrared.

Paper 21078 received Sep. 21, 2021; accepted for publication Jan. 27, 2022; published online Feb. 14, 2022.

1 Introduction

Over the years, optical overlay metrology has seen significant innovations that were needed to keep up with the demanding overlay requirements of the semiconductor industry. For many years, image-based overlay metrology using box-in-box metrology targets has been the work horse on essentially all layers.¹ A big improvement in metrology precision and robustness came with the introduction of advanced imaging metrology targets where the box structures were replaced by gratings.

Another big step forward was the introduction of (micro) diffraction-based overlay metrology (μ DBO) where an overlay target consists of overlapping grating-pairs.²⁻⁴ These overlapping gratings are optically coupled, and as a result of this coupling, a small shift between the gratings (overlay) creates a small but measurable intensity variation in the diffracted light. The use of multiple grating-pairs with different intentional overlay bias in an overlay target allows an

*Address all correspondence to Perry van Schaijk, p.vschaijk@arcnl.nl

accurate determination of overlay from the measured diffracted intensities.⁵ An evolution of the μ DBO targets that is much less sensitive to stack variations was proposed previously.⁶ The use of multiple wavelengths in μ DBO has significantly improved process-robustness and allowed accuracy levels in the subnanometer range even in the presence of process variations.⁷⁻⁹ As a result, metrology using μ DBO-marks has become the standard for many overlay-critical layers in logic and memory devices.

However, in addition to improving precision, accuracy, and robustness, overlay metrology tools must also deal with decreasing signal levels. Several materials that are regularly used in semiconductor device manufacturing, such as amorphous carbon, are highly absorbing at visible wavelengths, resulting in a loss of overlay signal. Solutions such as topography-transfer and mark clear-out are sometimes used to still detect a signal from an overlay target that is buried underneath an absorbing layer. However, topography transfer is not always robust, and it can also introduce additional overlay metrology errors. Mark clear-out is also not preferred since it involves additional processing steps that increase cost.

A more preferred approach would be the use of (near) infrared wavelengths since many materials such as silicon and amorphous carbon tend to become more transparent toward longer wavelengths. However, enlarging the wavelength range of optical overlay metrology tools is far from trivial, since these tools contain many high-quality lenses that need antireflection (AR) coatings to minimize light losses and ghosting effects. The wavelength range of these AR coatings is usually limited to about one octave, which prevents a significant extension of the wavelength range of an optical metrology tool. Moreover, one would also need an image sensor that covers the visible to the infrared wavelength range and that also offers a high quantum efficiency and low read noise levels. Despite the impressive progress in image sensor technology, there is still a significant challenge to reach the low read noise levels in the infrared wavelength range.

One could consider, using dedicated overlay metrology tools for visible-only and infrared-only. From a technical perspective, this is possible but this will significantly raise the cost-of-metrology. Moreover, this is also not attractive in terms of ease-of-use. Ideally, one would like to have an overlay metrology tool that covers the full wavelength range from visible to infrared in a single sensor with the performance and cost level of existing tools.

In this paper, we present dark-field digital holographic microscopy (df-DHM) as a potential solution. Our df-DHM microscope offers a wavelength range of 400 to 1100 nm and uses only one uncoated lens for imaging an overlay target on an image sensor. The aberrations of this single lens can be computationally corrected using established backpropagation algorithms.¹⁰ Details of our df-DHM concept have been published previously¹¹ and here we extend our setup with an image sensor that offers a large wavelength range with high quantum efficiency but with somewhat elevated read noise levels¹² (Sony IMX990). However, the coherent detection in df-DHM raises even weak metrology signals well above the noise levels of this image sensor.

It should be noted that synthetic extensions of the wavelength range are possible using DHM.¹³ In such a system, a digital hologram is illuminated using two beams, each at a different wavelength. Each of these beams provides phase information about the object modulus its wavelength. By combining the phase information from both beams, it is then possible to define a synthetic beat wavelength as $\Lambda = (\lambda_1\lambda_2)/(\lambda_2 - \lambda_1)$, where λ_1 and λ_2 are the wavelengths of the two beams, respectively. While such a solution provides an excellent extension of the wavelength range when the object responds similarly to each individual wavelength, its use is limited when the object response depends on the wavelength. For example, amorphous silicon has an absorption coefficient of $17\,184\text{ cm}^{-1}$ at a wavelength of 800 nm, but is almost completely transparent at 1600 nm.¹⁴ This means that any object that is buried beneath a layer of amorphous silicon yields a weak signal at visible wavelengths and thus does not allow this wavelength to be synthetically extended. In the infrared, it is quite possible to image through the layer of amorphous silicon demonstrating the benefit of using longer wavelengths.

In the next section, we first briefly summarize our df-DHM concept followed by a description of the breadboard setup. We then present the first proof-of-concept data to demonstrate the potential overlay metrology capabilities of our df-DHM concept. We end the paper by identifying the major effects that are currently limiting performance and by proposing methods of solving these limitations.

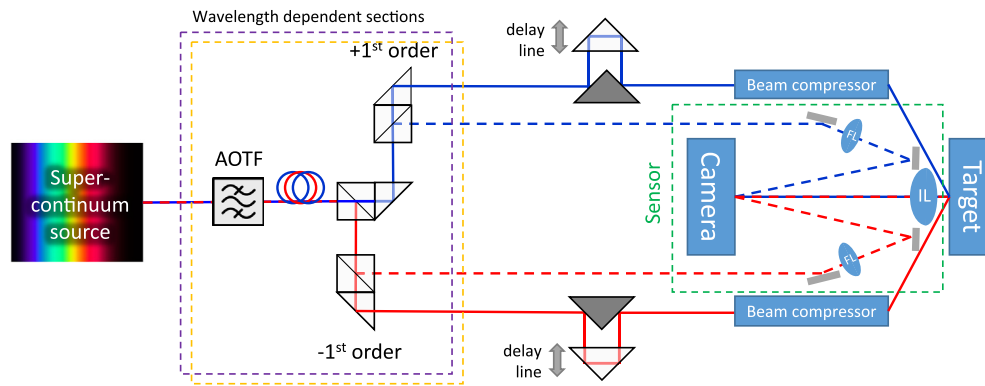


Fig. 1 Schematic representation of our df-DHM setup consisting of the actual sensor (highlighted in green) and the illuminator (rest of the setup). Light is generated using a supercontinuum source, filtered by an AOTF and split into four branches. The blue and red lines indicate the beam path of the beams corresponding to the +1st- and -1st diffraction orders, respectively. The solid lines indicated the illumination beams, while the dashed lines indicate the reference beams. A dark-field image is created using the imaging lens (IL). Finally, the reference beams are focussed next to the IL by a focussing lens (FL) such that the beam on the camera is diverging. The setup contains two AOTFs and two beam splitting sections as indicated in the figure by the dashed rectangle. Currently, switching between the two wavelength ranges is performed using flip-mirrors, but these can be easily replaced by dichroic mirrors.

2 Operating Principle

We propose to measure overlay (OV) of μ DBO gratings using a dark-field digital holographic microscope. Our df-DHM microscope has already been extensively reported previously¹¹ and is schematically shown in Fig. 1. The wafer is illuminated at an angle of 70° relative to the wafer normal using a polarized, collimated, and coherent beam of light. The dark-field is subsequently imaged onto a camera that is located above the wafer using a single imaging lens. Here, an off-axis hologram is created due to the coherent interference with a tilted reference beam. From this hologram, the complex electric field of the light at the camera plane can be recovered computationally as described in Ref. 11.

Since the complex electric field fully describes a polarized beam of light, the collected hologram can be used to computationally backpropagate the light, e.g., to the pupil plane. When the object is a point scatterer, the phase profile that is obtained in this plane is a good representation of the aberrations of the imaging lens. It is therefore possible to correct for the lens aberrations, e.g., by subtracting the phase profile that was measured for a point scatterer (the reference) from the profile that was measured for an overlay target. This technique is explained in detail in one of our earlier papers.¹⁰ As shown in this paper, excellent imaging performance can be achieved using this method even using a severely aberrated optic. Since the lens does not have to be well-corrected for aberrations a simple, single lens element can be used. This limits the number of air-glass interfaces and results in low reflection losses even without antireflective coatings. This eliminates the main reason for the limited wavelength range of most optics, and therefore the simple imaging lens can operate over a very wide wavelength range.

One other feature of our df-DHM concept is the parallel acquisition of the +1st and -1st order dark-field images of the μ DBO overlay targets.¹¹ As a result of this unique feature of DHM, we can use the full numerical aperture (NA) of the imaging lens, which helps to improve the spatial resolution, which is beneficial for small metrology targets. Moreover, a large imaging NA also offers a larger wavelength range over which a metrology target can be measured.

3 Experimental Setup

The experimental setup consists of two parts: an illuminator that generates and conditions the two illumination and reference beams and a sensor that collects the actual holograms. Both are schematically shown in Fig. 1 and a photograph of the setup is shown in Fig. 2. Coherent light is

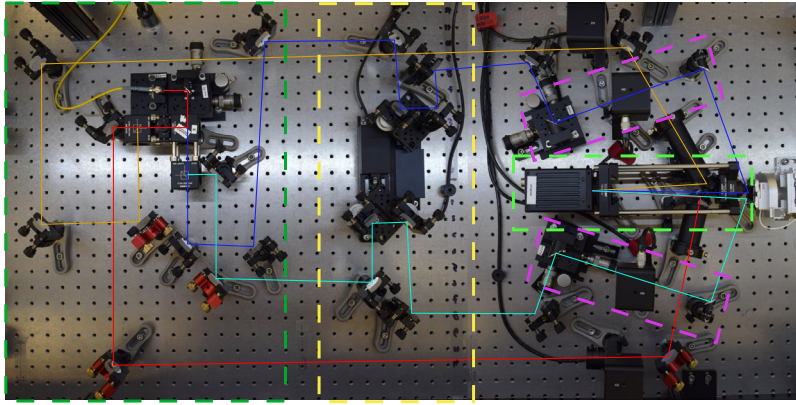


Fig. 2 Photograph of the experimental setup. Not included in the photo are the fiber-coupled supercontinuum source, the AOTFs and the beamsplitting cubes for the near-infrared wavelengths. Visible light arrives from the AOTF through the yellow fiber in the top left and is collimated using an OAPM. Then, a set of beam splitting cubes splits the beam into four, indicated in red, orange, blue, and cyan. After the splitting section (dashed dark green box), two delay lines ensure path length matching (yellow box). Subsequently, two beam compressors consisting of OAPMs reduce the beam size of the illumination beams (magenta boxes). Finally, the dark field of the overlay targets is imaged onto a camera in the actual sensor (light green box). The photo is mirrored in the horizontal direction to match the schematic in Fig. 1.

generated using a supercontinuum laser spanning a bandwidth of 410 to 2400 nm (Leukos Rock 400 5). Subsequently, the light is spectrally filtered using two acousto-optic tunable filters (AOTFs) (Leukos Tango Dual VIS-NIR1). These AOTFs cover wavelength ranges of 400 to 650 nm and 640 to 1100 nm, respectively. Each of the AOTFs is fiber coupled to an endlessly single mode photonic crystal fiber and the output of each of these fibers is collimated using an off-axis parabolic mirror (OAPM) that operates over a very wide wavelength range (Thorlabs MPD01M9-P01). Next, the two beams are split into four beams using a set of beam splitter cubes optimized for each respective wavelength range with a 45%–45%–5%–5% splitting ratio. A set of flip-mirrors then allow to select between the two operating ranges. It should be noted that this beam combining can also be done using dichroic mirrors to eliminate this mechanical step. Finally, the two illumination beams each pass through a separate optical delay line matching the optical path length of the illumination beam to its corresponding reference beam to well within the coherence length of the light source, ensuring interference at the camera plane. The resulting four beams propagate to the sensor.

This sensor was already described in some detail in the previous section. The illumination beams pass through a beam compressor consisting of two OAPMs, allowing for a wide wavelength range. As a sample, we typically use a simple test wafer containing multiple μ DBO grating pairs as shown in Fig. 3. The dark field is imaged using a custom-made CaF_2 bispheic lens with a focal length of 4.283 mm and an NA of 0.5. This lens was optimized for a magnification of 50 \times and a wavelength of 400 nm, which minimizes the total aberrations over a bandwidth of 400 to 1100 nm.

The reference beams pass through a focusing lens. This lens focusses the beam onto a mirror adjacent to object beam and this serves two purposes. First, the center of the focussed spot can be closer to the object beam than that of a large beam. This significantly reduces the angle between the object and reference beams and therefore the fringe frequency on the camera and the requirement on the pixel pitch. Second, the imaging system is nontelecentric and therefore a spherical wavefront is projected on the camera. By matching the radius of curvature of the reference beam to that of the object beam, the recovery from the hologram improves. In our current setup, we use free-space coupling to project illumination beams on the wafer and the reference beams on the camera. However, we have shown previously¹¹ that we can also use fiber coupling which we will implement as one of the next steps in this investigation.

Finally, the beams interfere at the camera (Aval ABA-013VIR-GE, Sony IMX990 sensor). This camera has a relatively uniform quantum efficiency ranging from 400 to 1600 nm. This is

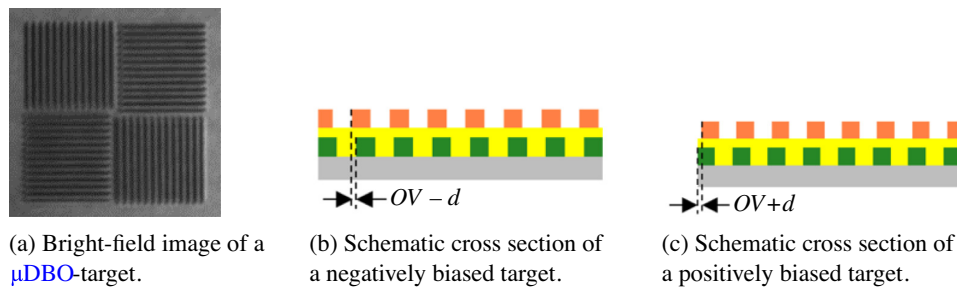


Fig. 3 (a) A μ DBO-target consists of four grating pairs. Two of these grating pairs run in the vertical direction and are used to measure overlay in the horizontal direction, the other two grating pairs are used to measure overlay in the vertical direction and are not used in this paper. (b), (c) A cross-section of the two vertical grating pairs. As can be seen, each of the grating pairs has an intentional offset in the overlay of $d = 20$ nm. By measuring both gratings pairs, the measurement can be made independent of the stack in between the top and bottom gratings.

achieved by thinning down the InP substrate of a backside-illuminated InGaAs camera sensor. In addition, this sensor features a pixel pitch of $5 \mu\text{m}$, which is achieved by replacing the typical In-bump that connects the photosensitive die to the readout electronics by Cu–Cu bonds. Both features have been industrialized relatively recently and play a crucial role in enabling holography from the visible to infrared using a single sensor.

4 Signal Processing

After capturing the hologram on the camera, all processing is done computationally. These steps were explained in great detail in Ref. 11 and will be covered more briefly in this section. All images in this section were obtained at a wavelength of 520 nm. For each additional wavelength of interest, we repeat the entire procedure.

As an input to the algorithm, two images are required: a hologram of the target and a hologram of a reference grating, which allows calibration of the beam profile of the illumination beam. This reference grating would normally be on a fiducial, but for this first experiment we used a resist-only grating that was present on our wafer sample. The signal flow is schematically shown in Fig. 4. Each of these holograms is first converted to the spatial frequency domain using a Fourier transform (FFT), resulting in images such as Fig. 4(c). Subsequently, the two sidebands are computationally filtered and shifted to the baseband.

Then, an inverse FFT (iFFT) is performed to obtain the two dark-field images corresponding to the two diffraction orders, which are shown in Figs. 4(b) and 4(d). In these images, we can then define a region of interest for each of the biased gratings and integrate the power in each of these gratings. This yields four values for the target hologram and four values for the reference hologram. To make the system less susceptible to inhomogeneities in the illumination beam, the target values are divided by their corresponding reference value. Finally, the asymmetry in the diffraction pattern is calculated and the OV is calculated from these asymmetries as is typically done for μ DBO-targets.

5 Results

To demonstrate the wide wavelength range of operation for the sensor, we show images of μ DBO targets ranging from 500 to 1100 nm in Fig. 5. As shown in Fig. 5(a), the sensor captures multiple diffraction orders at shorter wavelengths. At longer wavelengths, the diffraction orders pass through the edge of the NA and aberrations start to become more apparent. This is especially apparent in Fig. 5(e). Such aberrations can be corrected using the procedure outlined in Ref. 10, but this is outside the scope of this paper.

To demonstrate the wide bandwidth of operation further, we used this setup to measure the OV of a range of μ DBO targets with a programmed overlay of -20 , -10 , 0 , 10 , and

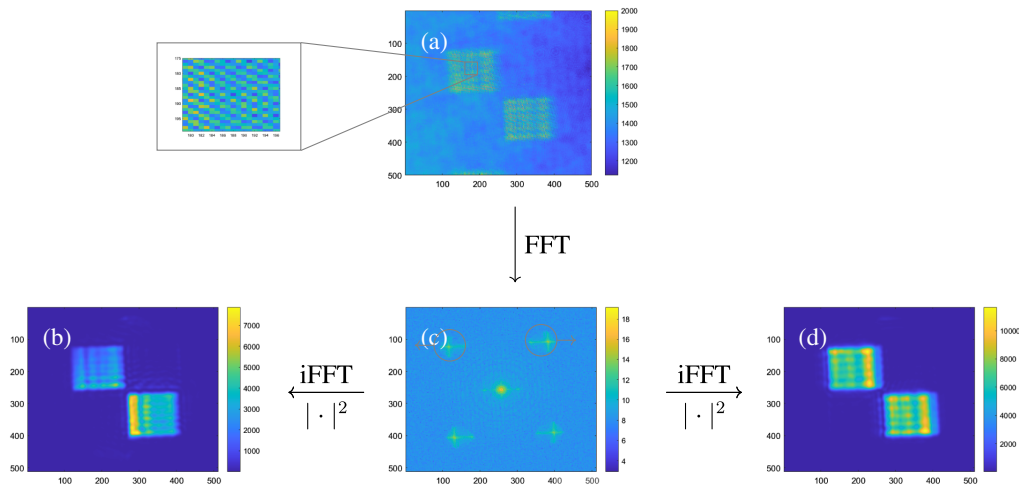


Fig. 4 Signal flow for the reconstruction. (a) The raw camera image and the zoomed image clearly shows that the fringes of the hologram are resolved. After performing an FFT, it is clear that the signal is split into a baseband and four sidebands in (c). The baseband is not of interest to us, but the sidebands contain the complex electric field of the +1st and -1st diffraction orders. Each sideband is separately filtered using the window shown, shifted to the baseband, and converted back to image space using an iFFT. Finally, the absolute squared value is taken to obtain an image similar to a regular dark-field image, but with the advantage that both diffraction orders can be measured simultaneously and that the phase-image is also retrieved. The resulting image for the -1st and +1st diffraction orders are shown in (b) and (d), respectively.

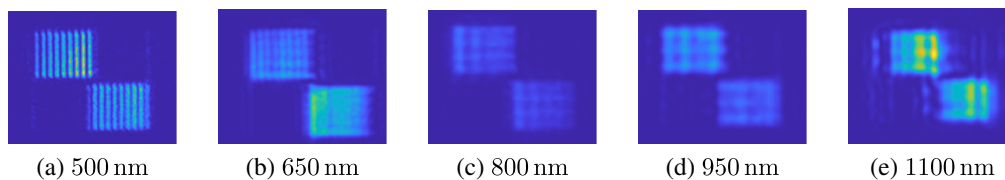


Fig. 5 Demonstration of the wide wavelength range over which the sensor can operate. Each of the images shows a 900-nm-pitch μ DBO-target measured at the indicated wavelength. Each of the gratings is $8 \times 8 \mu\text{m}^2$.

20 nm. The resulting measured overlay values are shown for each programmed overlay value in Figs. 6(a) and 6(b) for a wavelength of 520 and 1100 nm, respectively. These wavelengths were also chosen because they clearly demonstrate the potential to provide visible to infrared overlay measurements using a single sensor. It should be noted that the target used for the measurement at $\lambda = 520$ nm showed a stack sensitivity of 0.59, whereas target used at $\lambda = 1100$ nm showed a stack sensitivity of 0.12. Since stack sensitivity is a measure for the asymmetry in the diffraction pattern as a function of overlay, this means that the measured asymmetry and thus the signal-to-noise ratio is almost five times greater for the same overlay value for the $\lambda = 520$ nm target as compared with the $\lambda = 1100$ nm target. This explains the difference in performance for these two wavelengths.

In these figures, it can be clearly seen that the sensor is sensitive for wavelengths ranging from the visible to the infrared. Large errors are still present, however, due to a combination of low stack sensitivity, poor focus control, and a poor beam quality in combination with oblique illumination. In addition, the sensor is sensitive to phase fluctuations and therefore to air turbulence, which also affects the static reproducibility, as shown in Fig. 7.

The 3σ -deviation was determined to be 122 and 76 pm for the $\lambda = 520$ nm and $\lambda = 1100$ nm measurements, respectively. The stability of the current breadboard setup can still be improved substantially by a reduction of the optical path lengths and by physically shielding the beams from air turbulence.

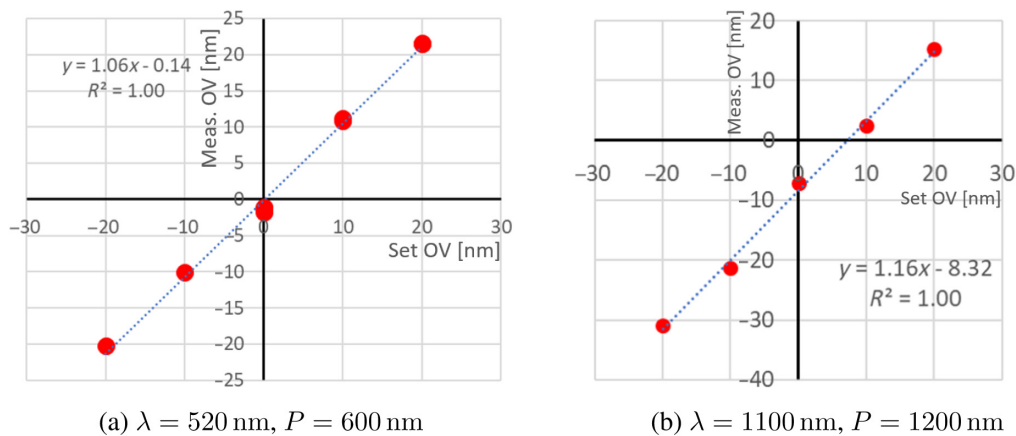


Fig. 6 Measured overlay versus the expected overlay for wavelengths (λ) of 520 and 1100 nm. The grating pitch (P) was selected such that the diffracted light would be close to the center of the pupil for minimum aberrations. These constitute the first-ever overlay measurements ranging from the visible to the infrared with a single sensor. As can be seen, performance is slightly worse in the infrared. This is not inherent to the wavelength, but to the sample that we used as is explained in the text.

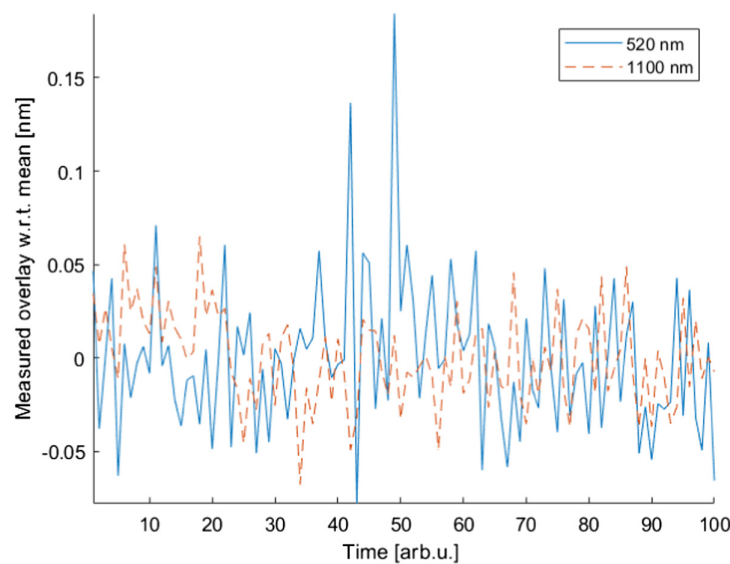


Fig. 7 Static reproduction of the overlay with respect to its mean value for 600 and 1200 nm pitch targets measured at a wavelength of 520 and 1100 nm, respectively. After preparing the setup, 100 camera images were acquired without intentionally changing the setup in any way. Any fluctuations in the measured overlay value therefore represent noise which we attribute to mechanical instabilities and turbulence.

Finally, it is worthwhile to note that Si becomes transparent above 1030 nm. This means that a significant fraction of the light propagates to the back of the wafer, reflects off the sample holder, and propagates back to the camera. This is most apparent when comparing a regular dark-field image obtained at 1030 nm to one obtained at 1100 nm as shown in Figs. 8(a) and 8(b), respectively. Fortunately, the coherence length of the light that we use is much shorter than the thickness of the sample, meaning that the reflected light does not interfere with the reference beam. From a hologram obtained at 1100 nm, it is therefore possible to recover the dark-field image using the process shown in Fig. 4. The result is shown in Fig. 8(c) and it is indeed clear that the background is much darker.

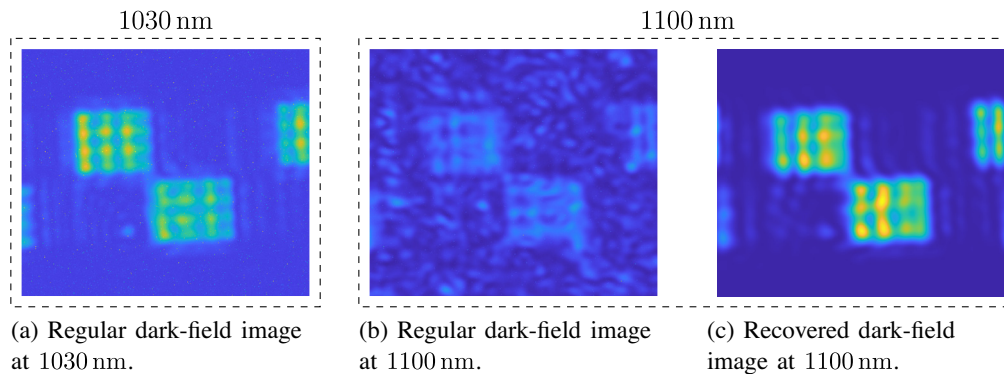


Fig. 8 Demonstration of the power of coherence gating at infrared wavelengths. Up to a wavelength of 1030 nm Si is opaque and good images can be obtained using a regular dark-field microscope as is shown in Fig. 8(a). For longer wavelengths, Si becomes transparent which allows the light to propagate to the backside of the wafer. This results in a strong background signal as is shown in Fig. 8(b). DHM is only sensitive to signals with an optical path length that match the optical path length of the reference beam due to coherence gating. By carefully matching the optical path length for light diffracted of the front side of the wafer, the background can be suppressed quite substantially as shown in Fig. 8(c).

6 Conclusion

In conclusion, we have demonstrated for the first time a single sensor for measuring overlay on semiconductor wafers from the visible up to the near-infrared. The sensor operates based on digital holographic microscopy and is able to obtain the overlay values using a single image acquisition, while at the same time allowing the use of the full NA of the lens. A good correlation between programmed and measured overlay was found.

In the future, the wavelength range of the sensor can be extended even further by including an additional AOTF operating up to the maximum wavelength covered by the camera, 1600 nm. In addition, the stability of the measurements can be increased by enclosing the beam to avoid air turbulence and by increasing the region with good fringe contrast by reducing the bandwidth of the source and by path length matching the illumination beam to the reference beam coming from the opposite side of the sensor. Another interesting addition to the sensor is the aberration correction technique,¹⁰ which will increase the image quality and remove the need for mechanical refocusing. Finally, many other technical improvements are envisioned to make the sensor more suited to an industrial setting. DHM therefore provides an interesting route toward the next generation of overlay sensors.

Acknowledgments

The authors wish to acknowledge the research group of Lyuba Amitonova for the many fruitful discussions, Bartjan Spaanderman for his technical assistance, and Marco Konijnenburg for the software that automates experiments. The authors N. Pandey, A. Koolen, and A. den Boef were employed by ASML while the research was conducted. T.T.M. van Schaijk joined the company after the research was concluded, but during the submission process of the paper. ASML has a commercial interest in overlay metrology.

References

1. M. Adel et al., "Optimized overlay metrology marks: theory and experiment," *IEEE Trans. Semicond. Manuf.* **17**(2), 166–179 (2004).
2. W. Yang et al., "A novel diffraction based spectroscopic method for overlay metrology," *Proc. SPIE* **5038**, 200–207 (2003).
3. M. Adel et al., "Diffraction order control in overlay metrology: a review of the roadmap options," *Proc. SPIE* **6922**, 692202 (2008).

4. P. Leray et al., "Diffraction based overlay metrology: accuracy and performance on front end stack," *Proc. SPIE* **6922**, 69220O (2008).
5. A. J. Den Boef, "Optical wafer metrology sensors for process-robust CD and overlay control in semiconductor device manufacturing," *Surf. Topogr. Metrol. Prop.* **4**(2), 023001 (2016).
6. M. Matsunobu et al., "Novel diffraction-based overlay metrology utilizing phase-based overlay for improved robustness," *Proc. SPIE* **11611**, 1161126 (2021).
7. H.-J. H. Smilde et al., "Evaluation of a novel ultra small target technology supporting on-product overlay measurements," *Proc. SPIE* **8324**, 83241A (2012).
8. K. Bhattacharyya et al., "Holistic approach using accuracy of diffraction-based integrated metrology to improve on-product performance, reduce cycle time, and cost at litho," *Proc. SPIE* **9424**, 94241E (2015).
9. K. Bhattacharyya et al., "A study of swing-curve physics in diffraction-based overlay," *Proc. SPIE* **9778**, 97781I (2016).
10. C. Messinis et al., "Aberration calibration and correction with nano-scatterers in digital holographic microscopy for semiconductor metrology," *Opt. Express* **29**(23), 38237–38256 (2021).
11. C. Messinis et al., "Diffraction-based overlay metrology using angular-multiplexed acquisition of dark-field digital holograms," *Opt. Express* **28**(25), 37419 (2020).
12. S. Manda et al., "High-definition visible-SWIR InGaAs image sensor using Cu–Cu bonding of III-V to silicon wafer," in *IEEE Int. Electron Devices Meeting*, pp. 16.7.1–16.7.4 (2019).
13. T. Colomb et al., "Automatic procedure for aberration compensation in digital holographic microscopy and applications to specimen shape compensation," *Appl. Opt.* **45**(5), 851–863 (2006).
14. D. T. Pierce and W. E. Spicer, "Electronic structure of amorphous SI from photoemission and optical studies," *Phys. Rev. B* **5**, 3017–3029 (1972).

Theodorus T. M. van Schaijk (PhD 2019, TU Eindhoven) is a researcher at ASML. Previously, he has worked on overlay metrology using digital holographic microscopy at the Advanced Research Center for Nanolithography (ARCNL) in Amsterdam. In 2019, he received his PhD in integrated optics in 2019 from the Eindhoven University of Technology for his work on a feedback insensitive integrated semiconductor laser. His interests include overlay metrology and other topics related to metrology used in semiconductor fabrication.

Christos Messinis is currently a PhD employee at the ARCNL on the Computational Imaging Group. The goal of his research is the development of a metrology tool based on holography, capable of robust semiconductor metrology on a large wavelength range (400 to 1600 nm) with sub-nm precision. He received his BSc degree in material science and his MSc degree on photonics-lasers from the University of Patras, Greece.

Nitesh Pandey (PhD 2011, NUI Maynooth) is a principal research engineer working at the Advanced Technology Development Group at ASML. He is currently working on topics related to pattern fidelity and semiconductor process control such as reticle metrology, overlay metrology, and stochastic EPE modeling.

Armand Koolen (PhD 2000, TU Eindhoven) is a principal researcher in ASML, primarily involved in optical metrology, such as the YieldStar optical scatterometer for overlay, focus, and critical dimension determination.

Stefan Witte (PhD 2007, Vrije Universiteit Amsterdam) is a group leader of the EUV generation and Imaging Group at ARCNL, head of the ARCNL Metrology Department, and associate professor at the Vrije Universiteit Amsterdam. His research interests include coherent diffractive imaging with visible and EUV radiation, high-harmonic generation and its applications, photo-acoustic imaging, and advanced laser development for plasma experiments.

Johannes F. de Boer is a full professor in the Department of Physics and Astronomy of the Vrije Universiteit, Amsterdam, the Netherlands. His research focuses on optical coherence tomography and light interferometry for biomedical imaging and metrology in scattering samples, and the characterization of local polarization properties.

Arie den Boef received his degree in electrical engineering from the Eindhoven Polytechnic Institute and his PhD from the University of Twente. He has been with Philips from 1979 to 1997 where he has worked in the area of laser diodes, optics, MRI and optical storage. He joined ASML in 1997, where he has explored various optical metrology techniques. He is also a part-time full professor at the Vrije Universiteit of Amsterdam.